The gyromagnetic Fabry-Pérot resonator: II. Dipole-exchange effects

1998 J. Phys.: Condens. Matter 10 1891

(http://iopscience.iop.org/0953-8984/10/8/021)

J. Phys.: Condens. Matter **10** (1998) 1891–1907. Printed in the UK PII: S0953-8984(98)86149-3

The gyromagnetic Fabry–Pérot resonator: II. Dipole-exchange effects

Siew-Choo Lim†, Junaidah Osman† and D R Tilley†‡

† School of Physics, Universiti Sains Malaysia, 11800USM, Penang, Malaysia
‡ Department of Physics, University of Essex, Colchester CO4 3SQ, UK

Received 15 July 1997, in final form 18 November 1997

Abstract. The transmission of electromagnetic radiation at normal incidence through a magnetic film is considered for film thickness L small enough to require the inclusion of exchange effects arising from the wave-number component $k_z \sim \pi/L$. We apply the continuum form of the dynamical equations with parametrized spin boundary conditions including pinned and unpinned spins as special cases. For applied field normal to the interfaces (Faraday geometry) the propagating modes are circularly polarized but because of the exchange there are two modes, say optical and spin, in each polarization. Equations for the transmission are given in a general form that allows for partial mirrors at the interfaces and applies to a film on a substrate as well as a free-standing film. Computed transmission spectra show that spin-wave fringes are unlikely to be observable for ferromagnets but can be significant in antiferromagnets. Some discussion is given of the implications for the characterization of antiferromagnetic film systems by means of far-infrared spectroscopy.

1. Introduction

In a previous paper [1], denoted I, we gave a preliminary discussion of the properties of a Fabry–Pérot resonator with a gyromagnetic medium between the partial mirrors. Two simplifications were made: exchange effects were not included because the permeability tensor μ was taken with no dependence on wave vector k and the problem was treated for the linear régime. These assumptions are practical for both ferromagnets and antiferromagnets provided that the thickness L of the resonator is such that $k \approx 1/L$ is not too large and that the incident intensity is not large. In I we discussed and illustrated the results for both Faraday (static field normal to mirrors) and Voigt (field in plane) geometries. In the former the optical eigenmodes are the circular polarization states; in terms of these in both ferromagnets and antiferromagnets normal-incidence transmission fringes are seen except near resonance where the medium is highly absorptive. The formalism allows for partially reflecting mirrors at the surfaces of the magnetic medium and the transmission peaks become sharper with increasing mirror reflectivity.

We extend these calculations by including exchange in the continuum approximation with the result that $\boldsymbol{\mu}$ becomes spatially dispersive because of a term Dk^2 in the denominator. For the Faraday geometry with normally incident radiation, which is all we discuss, the circular polarization states are still eigenmodes but there are now two possible values of k so from the optical point of view the medium is birefringent in either polarization. For practical values of D the two values of k differ greatly in magnitude and for most frequencies they can be regarded as an 'optical' mode k_O and a 'spin-wave' mode k_S with $k_S \gg k_O$.

0953-8984/98/081891+17$19.50

Because of the birefringence, calculation of transmission and reflection involves allowing for two downward and two upward waves in the medium. The standard electromagnetic boundary conditions are insufficient to determine all the coefficients and therefore 'spin' boundary conditions on the rf magnetization must be included. We take these in the standard Rado–Weertman [2] form that includes both pinned and unpinned spins as special cases.

Spin-wave fringes, which depend significantly on the form of the boundary conditions, are seen for $L \sim 1/D^{1/2}$. For a ferromagnet, with resonance wavelength λ_R in the microwave region, this means that $L \ll \lambda$. Thus the volume of magnetic material is very small on the scale of the wavelength and in consequence we find that the spin-wave fringes are far too small to be observable. Nevertheless, we include an illustration for two reasons. First a ferromagnet is the easiest example and second the obvious way to increase the magnetic volume is to consider a superlattice; the present calculation is a starting point for a study of transmission through a superlattice in the dipole-exchange régime. For an antiferromagnet, on the other hand, with λ_R generally some orders of magnitude larger than in a ferromagnet, the disparity between L and λ is not so great and in consequence the spin-wave fringes are on a practical scale. Furthermore, as mentioned, the form and scale of the fringes depends on the spin-wave boundary conditions so in principle the Fabry–Pérot resonator has potential application in the characterization of antiferromagnet film systems.

A general discussion of related literature was given in I and will not be repeated. However, we draw attention to two papers. Dipole-exchange effects in antiferromagnets were discussed by Stamps and Camley [3]. Their starting point is similar to ours but they go on to discuss the different problem of propagating dipole-exchange modes in a thin film. Lui *et al* [4] succeeded in observing spin-wave fringes in a microwave absorption experiment on epitaxial MnF_2 films of MBE quality.

In section 2 we derive the required forms of $\boldsymbol{\mu}$ and show some dispersion graphs, ω versus k. Section 3 is concerned with the optical problem of reflection and transmission. We show that an extension of the standard calculation enables the results for the Fabry–Pérot resonator to be expressed in terms of coefficients for reflection and transmission at a single interface. These coefficients are given in an appendix in general form. Computed graphs of transmission are shown and discussed in section 4. Finally, section 5 contains a general discussion and conclusions.

2. Susceptibilities and dispersion graphs

2.1. Ferromagnets

The central quantity is the susceptibility tensor $\chi(k,\omega)$ relating the rf magnetization $\boldsymbol{m}(\omega)$ to the incident rf field $\boldsymbol{h}(\omega)$; in the later optical calculations we use the permeability $\mu(k,\omega) = \mathbf{I} + \chi(k,\omega)$. These quantities can be derived from torque equations of motion [5] or from the continuum limit of microscopic equations [6]. We follow the latter route and include a Landau–Lifshitz damping term $-G_{LL}\boldsymbol{m} \times (\boldsymbol{m} \times \boldsymbol{H})$. Like the simpler dipolar equations [1] the equations of motion are diagonalized by the transformation $m^{\pm} = m^x \pm \mathrm{i}m^y$. Eventually we find for the corresponding susceptibilities

$$\chi^{\pm} = \frac{(1 \pm \mathrm{i}\eta)\omega_m}{(\omega_d + \omega_A + Dk^2)(1 \pm \mathrm{i}\eta) \pm \omega} \tag{1}$$

where $\omega_m = \gamma\mu_0 M_0$, with M_0 the static magnetization, $\omega_A = \gamma\mu_0 H_A$, where H_A is the anisotropy field, and $\omega_d = \gamma\mu_0 H_d$, where $H_d = H_0 - M_0$, which includes a demagnetization correction to the applied field H_0 since we take the field normal to the interfaces. The

damping parameter is $\eta = M_0 G_{LL}/\gamma\mu_0$ and D is related to the exchange constant J by $D = SJa^2/2$ with a the nearest-neighbour distance. We have made the replacement $\nabla^2 \rightarrow -k^2$ since we deal throughout with plane waves $\exp[\mathrm{i}(kz - \omega t)]$. Usually for ferromagnets the anisotropy ω_A can be neglected and when also $D \rightarrow 0$ (1) reduces to the well known form [1] for dipolar modes.

It helps in discussing Fabry–Pérot transmission and other optical properties to be able to refer to dispersion curves of ω versus k. The equation is

$$k^2 = \varepsilon\mu\omega^2/c^2 \tag{2}$$

with superscript $\pm$ implied on k and μ. Substitution of (1) into (2) gives a quadratic equation for k^2. The leading term is Dk^4 and since D is small we can use the fact that the roots of the quadratic equation $Dk^4 + bk^2 + c = 0$ are approximately $k^2 = -b/D$ and $k^2 = -c/b$. The first is the spin-wave and the second the optical mode mentioned earlier. The latter is quite well known since it is the purely electromagnetic mode and the explicit form of the former is

$$(k^{\pm})^2 = (\omega_m - \omega_0 \mp \omega)/D \tag{3}$$

in the approximation where damping is neglected.

Solutions of (3) are shown in figure 1 for $\omega_0 = \omega_m/2$ and $3\omega_m/2$. To a very good approximation the 'optical modes' are given by the permeabilities derived from (1) with $D = 0$ and figures 1(a) and 1(c) are readily understood on that basis. For $\omega_0 = \omega_m/2$, figure 1(a), μ^+ is resonant while μ^- is non-resonant and the dispersion curves are determined by these facts. Thus k_0^+ has a typical resonant form while k_0^- is predominantly imaginary for $\omega < \omega_m/2$ and real for $\omega > \omega_m/2$. For $\omega_0 = 3\omega_m/2$, on the other hand, it is μ^- that is resonant, as is reflected in figure 1(c). The 'spin modes' follow the approximate form (3) quite closely and it is easy to interpret figures 1(b) and 1(d) on the basis of (3). For $\omega_0 = \omega_m/2$, figure 1(b), k_S^+ is predominantly real for $\omega < \omega_m/2$ and imaginary for $\omega > \omega_m/2$ whereas k_S^- is predominantly real for all ω. The other important feature of figure 1 is the substantial difference in k scale between the optical and spin modes.

2.2. Antiferromagnets

The starting point is the Hamiltonian for a two-sublattice antiferromagnet with a static field directed along the easy axis, denoted z. In a subsequent section this will also be taken as the normal to the Fabry–Pérot mirrors. The Hamiltonian is

$$H = \sum_{\alpha,\beta} J_{\alpha,\beta}\boldsymbol{S}_\alpha \cdot \boldsymbol{S}_\beta - g\mu_B B_A \sum_\alpha S_\alpha^z + g\mu_B B_A \sum_\beta S_\beta^z - g\mu_B \boldsymbol{B}_a \cdot \left(\sum_\alpha \boldsymbol{S}_\alpha + \sum_\beta \boldsymbol{S}_\beta \right). \tag{4}$$

Here α refers to the spin-up and β to the spin-down sublattice. $J_{\alpha\beta}$ is the exchange interaction which favours antiparallel ordering of neighbouring spins. B_A is the effective anisotropy field, which has the same magnitude and opposite directions for the two sublattices. $\boldsymbol{B}_a$ is the applied field, defined as

$$\boldsymbol{B}_a = B_0\hat{\boldsymbol{z}} + b^x\hat{\boldsymbol{x}} + b^y\hat{\boldsymbol{y}} \tag{5}$$

with B_0 the applied static field, and $\boldsymbol{b} = b^x\hat{\boldsymbol{x}} + b^y\hat{\boldsymbol{y}}$ the rf driving field. There are no demagnetizing effects because without an external field the equilibrium magnetization in an antiferromagnet is zero.

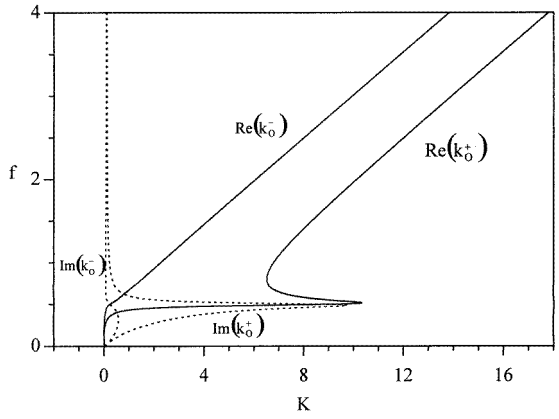

(a)

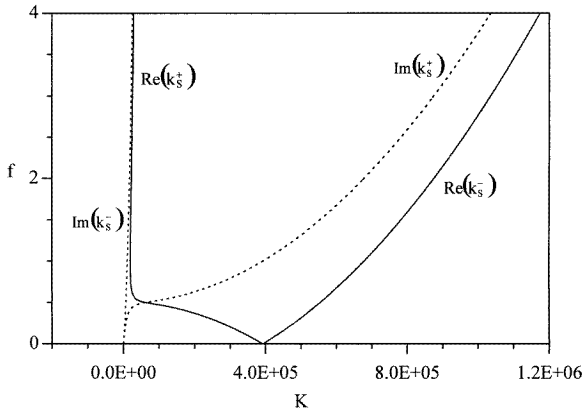

(b)

Figure 1. Dispersion curves for a YIG plate in normal magnetic field, propagation normal to plate (Faraday geometry). Parameters are $\mu_0 M_0 = 0.176$ T, $\varepsilon = 15.4$ and we assume $\omega_A = 0$ and $\Gamma = 0.05\omega_m$. (a) 'Optical modes' $k_O^{\pm}$ and (b) 'Spin modes' $k_S^{\pm}$ for $\omega_0 = \omega_m/2$; (c) 'Optical modes' $k_O^{\pm}$ and (d) 'Spin modes' $k_S^{\pm}$ for $\omega_0 = 3\omega_m/2$. Dimensionless variables are $f = \omega/\omega_m$ and $K = ck/\omega_m$.

The equation of motion for a spin operator is linearized by the RPA replacement $S^z \to S$ and continuum magnetization variables are introduced by the definition

$$\boldsymbol{m}(\boldsymbol{r}) = \upsilon_0 \boldsymbol{g}\mu_B \sum_i \boldsymbol{S}_i \delta(\boldsymbol{r} - \boldsymbol{r}_i) \tag{6}$$

where υ_0 is the number of spins per unit volume, $g\mu_B$ is the magnetic moment per spin, and $\upsilon_0 \sum_i \boldsymbol{S}_i \delta(\boldsymbol{r} - \boldsymbol{r}_i)$ defines an average over a volume containing many spins but with linear dimension small on the scale of variations of $\boldsymbol{m}(\boldsymbol{r})$. As in the case of the ferromagnet the resulting equations are diagonalized by the transformations $m^{\pm} = m^x \pm \mathrm{i}m^y$ for both sublattices. A Landau–Lifshitz damping term is includes for each sublattice and the final form of the equations is

$$[\omega + (\omega_0 + (\omega_E + \omega_A))(1 + \mathrm{i}\eta)]m_\alpha^+ = [-(\omega_E - Dk^2)(1 + \mathrm{i}\eta)]m_\beta^+ + [\omega_m(1 + \mathrm{i}\eta)]h^+ \tag{7}$$

$$[\omega + (\omega_0 - (\omega_E + \omega_A))(1 - \mathrm{i}\eta)]m_\beta^+ = [(\omega_E - Dk^2)(1 - \mathrm{i}\eta)]m_\alpha^+ + [-\omega_m(1 - \mathrm{i}\eta)]h^+ \tag{8}$$

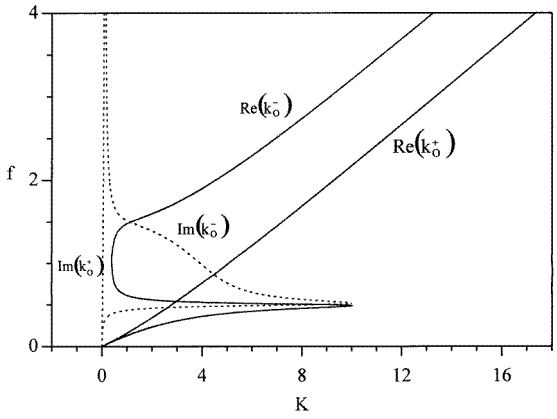

(c)

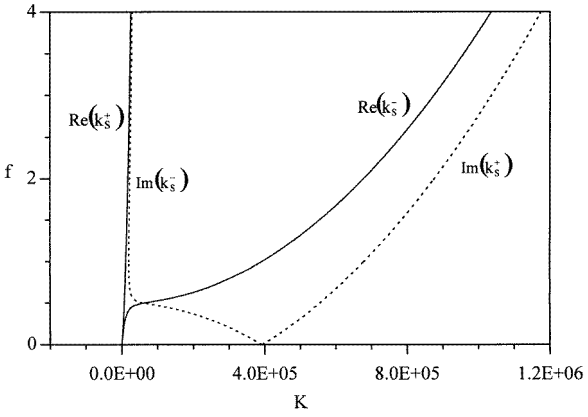

(d)

Figure 1. (Continued)

$$[\omega - (\omega_0 + (\omega_E + \omega_A))(1 - \mathrm{i}\eta)]m_\alpha^- = [(\omega_E - Dk^2)(1 - \mathrm{i}\eta)]m_\beta^- + [-\omega_m(1 - \mathrm{i}\eta)]h^- \quad (9)$$

$$[\omega - (\omega_0 - (\omega_E + \omega_A))(1 + \mathrm{i}\eta)]m_\beta^- = [-(\omega_E - Dk^2)(1 + \mathrm{i}\eta)]m_\alpha^- + [\omega_m(1 + \mathrm{i}\eta)]h^-. \quad (10)$$

Here η, ω_0, ω_A and ω_m are defined as for the ferromagnet with M_0 now the equilibrium sublattice magnetization. Now $D = SJa^2$ and $\omega_E = nSJ$ where n is the nearest-neighbour number and a the distance to nearest neighbours. The derivation of (7)–(10) is similar to that given by Stamps and Camley [3] in their discussion of dipole-exchange modes propagating in the plane of thin-film antiferromagnets. We note in particular that the effective field on sublattice α includes a term $D\nabla^2 m_\beta$ and vice versa.

The susceptibilities are defined by $m^\pm = \chi^\pm h^\pm$ where $m^\pm = m_\alpha^\pm + m_\beta^\pm$ and solution of (7)–(10) gives

$$\chi^\pm = \frac{-2\omega_m(\omega_A + Dk^2)(1 + \eta^2) + \mathrm{i}\{2\eta\omega\omega_m\}}{[\omega^2 \pm 2\omega\omega_0 + \{\omega_0^2 - (\omega_E + \omega_A)^2 + (\omega_E - Dk^2)^2\}(1 + \eta^2)] + \mathrm{i}\{2\eta\omega(\omega_E + \omega_A)\}}. \quad (11)$$

It is helpful for understanding later results to show the simplified form of $\chi^\pm$ obtained by putting $\eta = 0$ and dropping terms D^2k^4 in the denominator; reinstatement of the latter

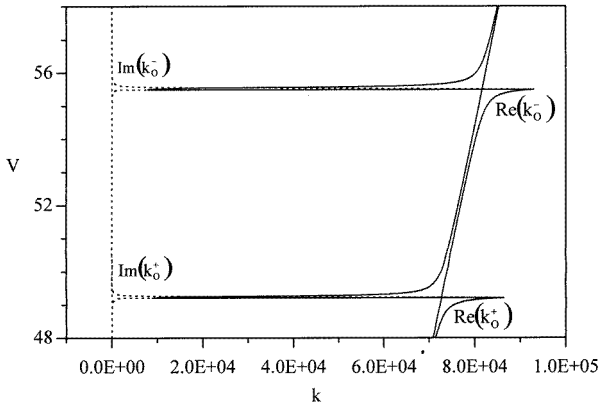

(a)

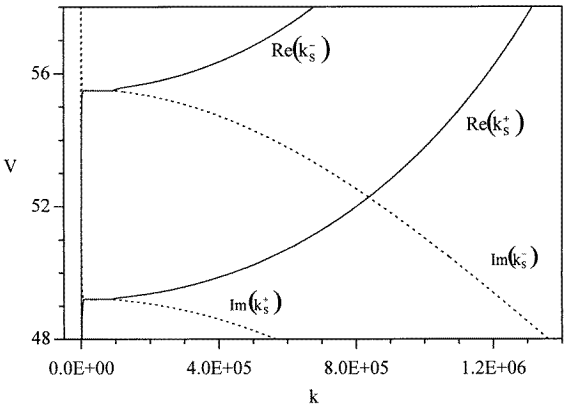

(b)

Figure 2. Dispersion curves for FeF_2 plate in normal magnetic field 3 T, propagation normal to plate (Faraday geometry). Axis variables are $V = \omega/2\pi c$ in cm^{-1} and k is in m^{-1}. Parameters are [7] $|M_{0\alpha}| = |M_{0\beta} = 0.056$ T, $\varepsilon = 5.5$, $B_E = 53.3$ T, $B_A = 19.7$ T, $D = 0.182 \times 10^{-6}$ rad s^{-1} m^2 and we take damping parameters $|\Gamma_\alpha| = |\Gamma_\beta| = 1.0 \times 10^{-4}\omega_m$. (a) Optical modes, (b) spin-wave modes.

leads to inclusion of a higher-order spin-wave mode that is unlikely to be detectable. The simplified expression is

$$\chi^{\pm} \approx \frac{2\omega_m(\omega_A + Dk^2)}{[-(\omega \pm \omega_0)^2 + \omega_R^2 + 2\omega_E Dk^2]} \tag{12}$$

where $\omega_R^2 = \omega_A(2\omega_E + \omega_A)$ gives the antiferromagnetic resonance frequency. This form of χ brings out the well known property [7] that χ^+ and χ^- coincide in zero field and that the effect of applying a field is to produce a Zeeman splitting $\pm\omega_0$.

The dispersion curves are given by (2) with $\mu^{\pm} = 1 + \chi^{\pm}$ and the general structure can be seen by inserting (12); it is adequate to take $\omega_0 = 0$ and therefore $\chi^- = \chi^+$ since the effects of Zeeman splitting are fairly obvious. Equations (2) and (12) lead to

$$2\omega_E Dk^4 + (\omega_R^2 - \omega^2)k^2 + (\varepsilon\omega^2/c^2)(\omega^2 - \omega_R^2 - 2\omega_m\omega_A) = 0 \tag{13}$$

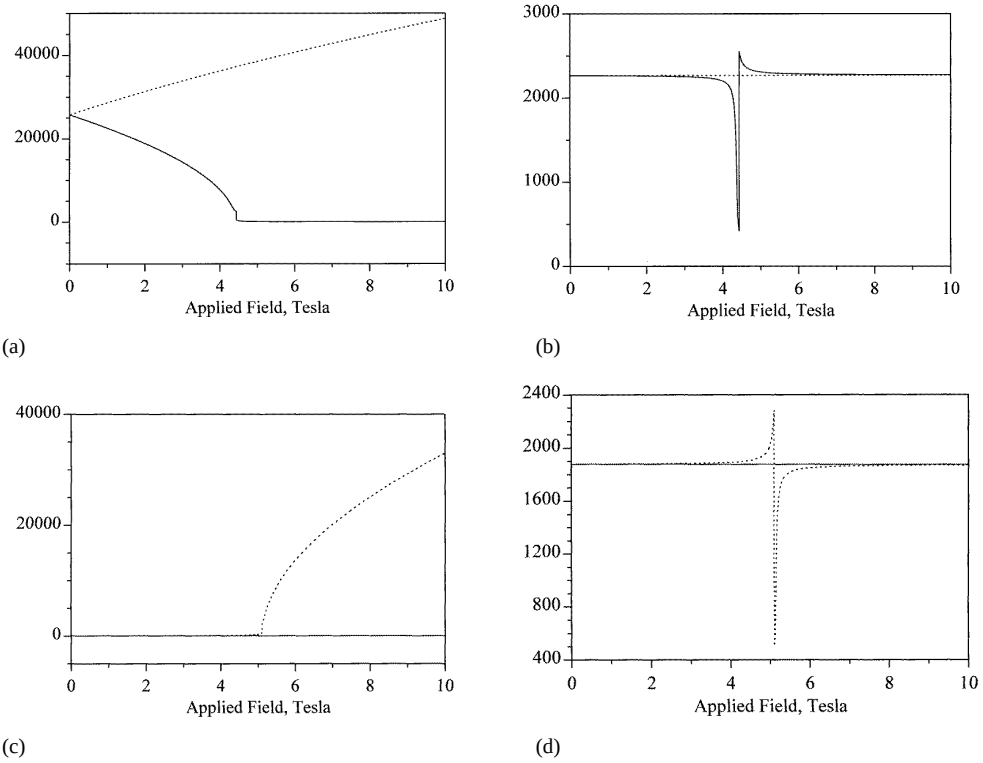

Figure 3. Dispersion curves for FeF_2 plotted as $k^+_{S,O}$ (– – –) and $k^-_{S,O}$ (——) in m^{-1} versus field at fixed frequency. Only real values of k are shown. (a) $\mathrm{Re}(k^{\pm}_S)$ and (b) $\mathrm{Re}(k^{\pm}_O)$ for $\omega/2\pi c = 57.0\ \mathrm{cm}^{-1} > \omega_R$; (c) $\mathrm{Re}(k^{\pm}_S)$ and (d) $\mathrm{Re}(k^{\pm}_O)$ for $\omega/2\pi c = 47.0\ \mathrm{cm}^{-1} < \omega_R$.

where small terms proportional to D have been omitted in the coefficient of k^2. As for the ferromagnet, for small D the roots correspond to an optical and a spin-wave mode given by

$$k_O^2 = \frac{\omega_R^2 + 2\omega_m\omega_A - \omega^2}{\omega_R^2 - \omega^2} \tag{14}$$

$$k_S^2 = (\omega^2 - \omega_R^2)/2\omega_E D. \tag{15}$$

Illustrative dispersion curves for FeF_2 are shown in figure 2. These are based on the full form (11) of the susceptibility but in fact they are described quite accurately by (14) and (15). The form of the 'optical' modes, figure 2(a), is well known since it underlies interpretation of far-infrared spectra of uniaxial antiferromagnets. One sees a Zeeman-split resonance with what amounts to a magnetic *reststrahl* between the frequencies given by vanishing of the denominator and the numerator in (14). The 'spin-wave' modes, figure 2(b), show the same Zeeman splitting. It is notable, as is clear from (15), that apart from the small effect of damping $k^{\pm}_S$ is imaginary below and real above the resonance frequency $\omega_R \pm \omega_0$. It can be seen too that although there is a difference in horizontal scales between figures 2(a) and 2(b) it is much less marked than for the ferromagnet. One reason for this is that the resonance frequency is much higher and k scales with the resonance frequency. A second reason is that although D is numerically small it is multiplied in (15) by the large factor ω_E.

In section 4 we show calculated curves for transmission through an antiferromagnetic film as a function of frequency at fixed field and also as a function of field at fixed frequency. Spin-wave fringes are seen where k_S is predominantly real so to connect with the second form of plot we conclude this section by briefly discussing the variation of k_S with ω_0 when ω is fixed. With field included, (15) is an equation for $k_S^{\pm 2}$ in which ω^2 is replaced by $(\omega \pm \omega_0)^2$. It is easy to see from this that for $\omega > \omega_R$ k_S^+ is always real whereas for $\omega < \omega_R$ k_S^+ is real only for $\omega_0 > \omega_R - \omega$. On the other hand, for $\omega > \omega_R$ k_S^- is real only for $\omega_0 < \omega - \omega_R$ while for $\omega < \omega_R$ k_S^- is never real. Graphs of $\mathrm{Re}(k_S^{\pm})$ versus ω_0 for FeF_2 for two frequencies are shown in figure 3.

3. Fabry–Pérot transmission and reflection: theory

We now turn to the main calculation of this paper with notation defined in figure 4. As implied there, we restrict attention to normal incidence and we use the circular polarization states, so that the superscript $\pm$ is implied on all field amplitudes and related coefficients. Compared with the simpler calculation when exchange effects are neglected, the main complication is the presence of two downward and two upward waves in the magnetic medium. Because of this, it is necessary to define boundary conditions on $\boldsymbol{m}(\boldsymbol{r})$ to supplement the usual electromagnetic boundary conditions and as mentioned we take these in the Rado–Weertman form [2]

$$\frac{\mathrm{d}\boldsymbol{m}}{\mathrm{d}z} - \xi \boldsymbol{m} = 0 \tag{16}$$

where ξ is proportional to the surface anisotropy constant [8]. Equation (16) may be derived by consideration of surface terms in a torque formulation [2, 9] or from the continuum limit of the equation of motion of a surface spin. We derive the general results using (16) but for illustrative illustrations we focus on the limiting forms $\boldsymbol{m} = 0$ as $\xi \to \infty$, usually called the pinned-spins condition, and $\mathrm{d}\boldsymbol{m}/\mathrm{d}z = 0$ for $\xi = 0$, unpinned spins. As in I, we allow for partial mirrors at the interfaces by means of the boundary condition

$$\Delta H_{\parallel} = \alpha E_{\parallel} \tag{17}$$

where

$$\alpha = \sigma_2 - \mathrm{i}\omega\varepsilon_0\varepsilon_2 \tag{18}$$

results from a thin sheet of two-dimensional conductivity σ_2 and dielectric constant ε_2.

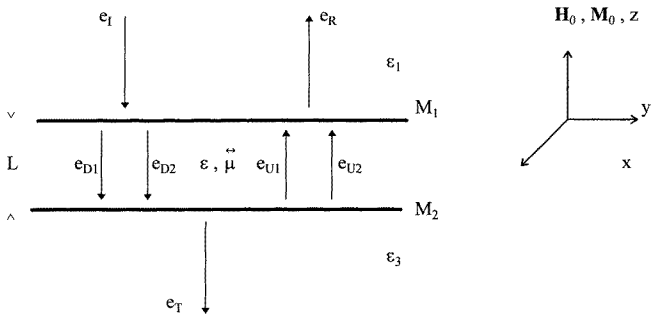

Figure 4. Notation for main calculation. We work in terms of the rf e fields and use the circular polarization states, with superscripts $+$ or $-$ implied on all field amplitudes e_I, e_R etc.

The coefficients for transmission and reflection of an ordinary Fabry–Pérot resonator can be found either by summation of the series arising from multiple reflections or by a resultant-wave method in which all the 'up' waves and all the 'down' waves are summed before electromagnetic boundary conditions are applied; the two methods can be shown to give the same results [10]. A useful refinement of the resultant-wave method results from the comment [11] that because of the linearity of the problem the boundary conditions can be written in terms of coefficients for the single interfaces. This is the method that is applied here. We define notation for the complex amplitude reflection coefficients ρ and transmission coefficients τ at the interface between medium 1 (isotropic dielectric) and 2 (magnetic medium) as follows, where for convenience we denote the modes in medium 2 simply as 1 and 2 rather than 'optical' and 'spin-wave' as before:

ρ_{12} is the ratio of the E-field reflected-wave amplitude to the incident-wave amplitude for the incident wave in 1 at the 1–2 interface.

ρ_{21ij}: incident and reflected waves in 2 with $i = 1, 2$ denoting the reflected wave and $j = 1, 2$ the incident wave.

τ_{12i}: incident wave in 1, transmitted in 2 of type i.

τ_{21i}: incident wave of type i in 2, transmitted in 1.

The explicit forms of these coefficients are given in the appendix and as stated we use them to write down the six boundary conditions for figure 4 in the form of linear equations relating each outgoing wave at each interface to the incoming waves. It is convenient to use the rf E Field amplitudes and in terms of these the boundary conditions are

$$e_R = \rho_{12}e_I + \tau_{211}e_{U1} + \tau_{212}e_{U2} \tag{19}$$

$$e_{D1} = \tau_{121}e_I + \rho_{2111}e_{U1} + \rho_{2112}e_{U2} \tag{20}$$

$$e_{D2} = \tau_{122}e_I + \rho_{2121}e_{U1} + \rho_{2122}e_{U2} \tag{21}$$

$$e_{U1} = \rho_{2311}\delta_{11}e_{D1} + \rho_{2322}\delta_{21}e_{D2} \tag{22}$$

$$e_{U2} = \rho_{2321}\delta_{12}e_{D1} + \rho_{2322}\delta_{22}e_{D2} \tag{23}$$

$$e_T = \tau_{231}\delta_{13}e_{D1} + \tau_{232}\delta_{23}e_{D2}. \tag{24}$$

In terms of phase factors $\phi_j = \exp(\mathrm{i}k_jL)$ corresponding to propagation of mode j across the magnetic region we have defined $\delta_{11} = \phi_1^2$, $\delta_{12} = \delta_{21} = \phi_1\phi_2$, $\delta_{22} = \phi_2^2$, $\delta_{13} = \phi_1$ and $\delta_{23} = \phi_2$.

Equations (19)–(24) together with the explicit forms of the single-interface coefficients given in the appendix are the main analytic results of this paper. These equations are quite general, applying to both ferromagnets and antiferromagnets. The superscript $\pm$ is implied on all relevant quantities so the result applies to both signs of circular polarization. The single-interface coefficients allow for general magnetization boundary coefficients in the form (16) and because of (17) and (18) they incorporate partial mirrors which may be absorbing ($\sigma_2 \neq 0$), pure dielectric and therefore energy-conserving ($\sigma_2 = 0$) or indeed absent ($\sigma_2 = 0$ and $\varepsilon_2 = 0$). Equations (19)–(24) also allow that media 1 and 3 may be different so that they apply, for example, to a film on a substrate as well as to a conventional Fabry–Pérot etalon in which these media are the same.

It is seen that (19)–(24) are six inhomogeneous linear equations giving the ratios to the incident field e_I of the six unknowns e_R, e_{D1}, e_{D2}, e_{U1}, e_{U2} and e_T of figure 4. We have used the algebraic manipulation package *Maple* to find the explicit solution for the complex transmission amplitude e_T/e_I but the result is not particularly illuminating and we do not show it here. In the computational work we used both of two slightly different methods. First we took the *Maple* expression for e_T/e_I and converted it automatically to Fortran code

and second we applied a standard numerical subroutine to solve (19)–(24) directly. These methods are not very different but use of both does give some check against trivial errors.

4. Transmission curves

We show here computed intensity transmission curves $|e_T/e_I|^2$ obtained by direct numerical solution of (19)–(24). Fringes related to the optical standing waves and governed by k_O were the subject of I so we now discuss only exchange-related fringes governed by k_S. The intention is to provide illustrative examples of the general results and we therefore simply consider transmission through a free-standing film so that media 1 and 3 are identical and we omit the effect of partial mirrors by putting $\alpha = 0$ in the boundary conditions (A2) and similar. For sufficiently large values of L the standing spin waves merge so that no fringes due to them can be seen in spectra. We have checked that for large L numerical results based on the full expressions presented here do coincide exactly with corresponding results from the programs used in I.

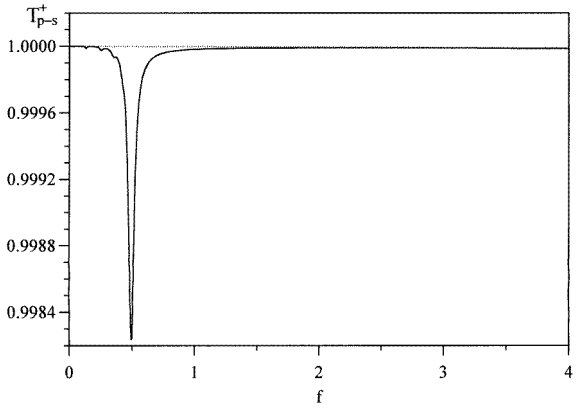

(a)

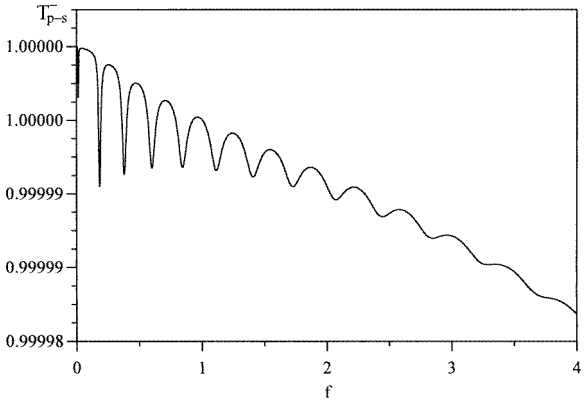

(b)

Figure 5. Transmission curves T versus $f = \omega/\omega_m$ for free-standing YIG film of thickness 1 μm with no mirrors. Pinned-spin boundary conditions were used. Applied field $H_0 = 0.5M_0$ and damping $\Gamma = 0.05\omega_m$. (a) + polarization and (b) − polarization.

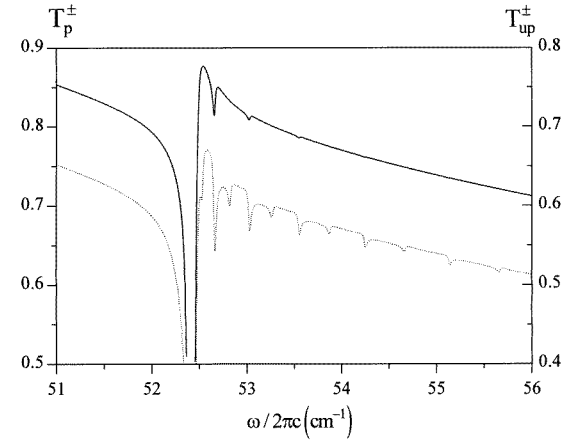

(a)

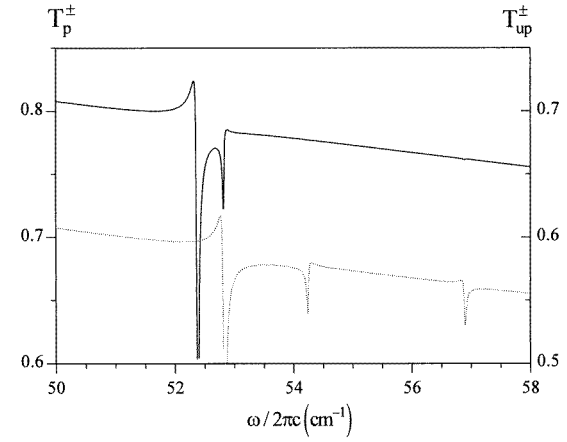

(b)

Figure 6. Frequency dependence of zero-field transmission through free-standing FeF_2 films of thickness (a) 50 μm and (b) 10 μm for pinned-spin (. . . and left-hand scale) and unpinned-spin (—— and right-hand scale) boundary conditions and damping $|\Gamma_\alpha| = |\Gamma_\beta| = 2.0 \times 10^{-4}\omega_m$.

The expectation for ferromagnets was that for spin-wave fringes to be seen the film would have to be very thin with the consequence that the magnetic volume is small and therefore the fringes are unlikely to be observable. This is indeed the case as is seen from the example in figure 5 where for simplicity we show the easily interpreted frequency scan. It is seen that even for pinned-spin boundary conditions the fringes are far too small to be observable and we found that they are smaller still for unpinned-spin boundary conditions. We show these results however because as mentioned it should be possible to generalize the formalism to superlattices in which the magnetic volume can be much larger.

We now turn to the more important case of antiferromagnets. The technique used by Lui *et al* [4] to observe spin-wave fringes on epitaxial MnF_2 films was cavity microwave absorption and the data take the form of derivative plots. In their nature, these cannot be converted into calibrated reflection or transmission curves so the only analysis possible is the determination of D from the fringe spacing; this is not a significant test of the theory

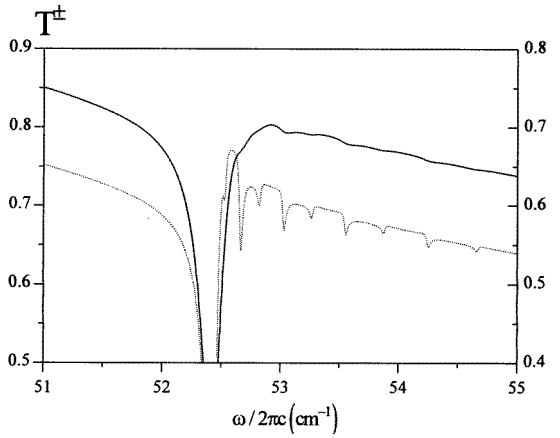

(a)

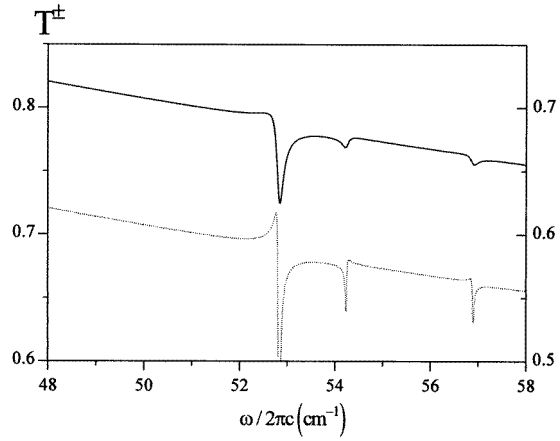

(b)

Figure 7. Frequency dependence of transmission through free-standing FeF_2 films of thickness (a) 50 μm and (b) 10 μm with pinned-spin boundary conditions for damping values $|\Gamma_\alpha| = |\Gamma_\beta| = 2.0 \times 10^{-4}\omega_m$ (... and left-hand scale) and $|\Gamma_\alpha| = |\Gamma_\beta = 10.0 \times 10^{-4}\omega_m$ (—— and right-hand scale).

presented here. As discussed in I, it is now possible to obtain high-quality frequency-swept spectra from high-resolution Fourier-transform instruments [7, 12, 13] and we concentrate on spectra of this kind since they can be compared in detail with theory [7]. We use the parameters of FeF_2 since the resonance frequency of 52 cm^{-1} falls in a convenient range. For simplicity, we discuss only free-standing films with no mirrors and as mentioned we compare the limiting cases of pinned- and unpinned-spin boundary conditions, $\xi \to \infty$ and $\xi = 0$ in (16).

Figure 6 shows the frequency dependence of transmission in zero field, $\omega_0 = 0$, for two films of thicknesses $L = 50$ and 10 μm. As seen from (11) χ^+ and χ^- coincide in this case so the curves apply to either sign of circular polarized radiation or indeed to unpolarized radiation. It is seen that the form of the fringe pattern depends strongly on the spin boundary conditions. The curves show spin-wave fringes of spacing given by $k_S L = n\pi$ superposed on a slowly changing background that results from the optical-wave fringes of spacing given

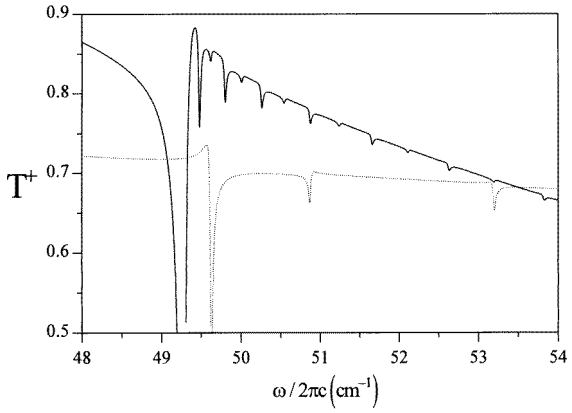

(a)

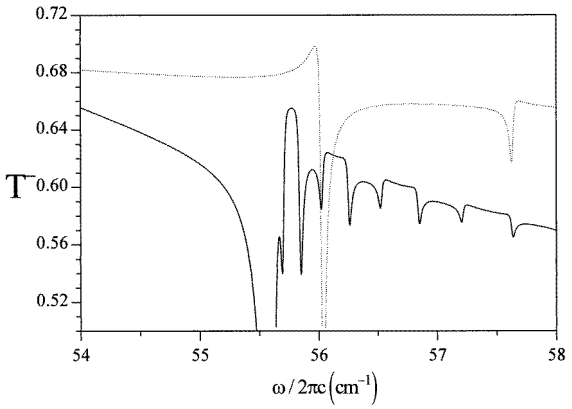

(b)

Figure 8. Frequency dependence of transmission through free-standing FeF_2 films with $|\Gamma_\alpha| = |\Gamma_\beta = 2.0 \times 10^{-4}\omega_m$ and thicknesses 50 (——) and 10 μm (. . .) with pinned-spin boundary conditions in applied field $H_0 = 3$ T. (a) + and (b) − circular polarization.

by $k_O L = n\pi$. In the immediate vicinity of the resonance frequency ω_R both sets of fringes are suppressed due to the strong absorption resulting from the strongly peaked $\mathrm{Im}(\chi)$. It is striking that the spin-wave fringes are present only for $\omega > \omega_R$; this is a consequence of the fact that k_S is real only for $\omega > \omega_R$, as seen in figure 2(b). The fringes for unpinned-spin boundary conditions are much less prominent than those for pinned spins. On the scale of figure 6 they are hardly discernible away from resonance although minor features can be seen in the data files.

It is to be expected that the form of the fringes depends strongly on damping and we illustrate this in figure 7 where it is seen that the fringes become broader and shallower as damping increases. Like those in figure 6, the zero-field transmission curves in figure 7 apply for unpolarized radiation. A further expectation is that if mirrors are included with an increase in partial reflectivity at the interfaces then the fringes will sharpen. We have not checked this although as noted partial mirrors are included in the formalism.

We have commented already that it follows from (11) and (12) that the effect of an applied field is to produce a Zeeman splitting $\pm\omega_0$ between the dispersion curves for + and

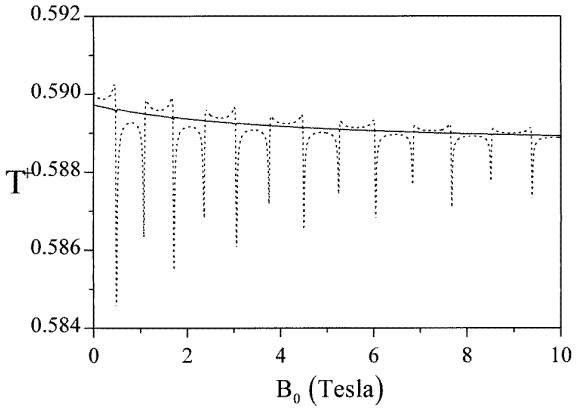

(a)

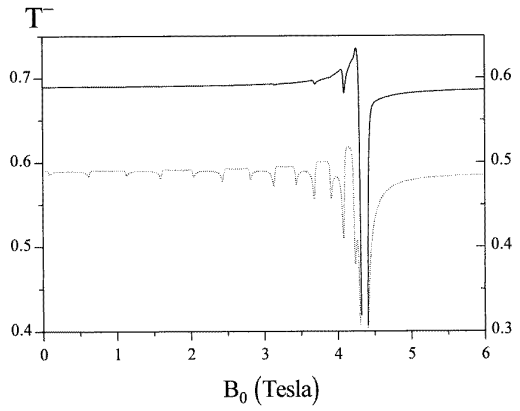

(b)

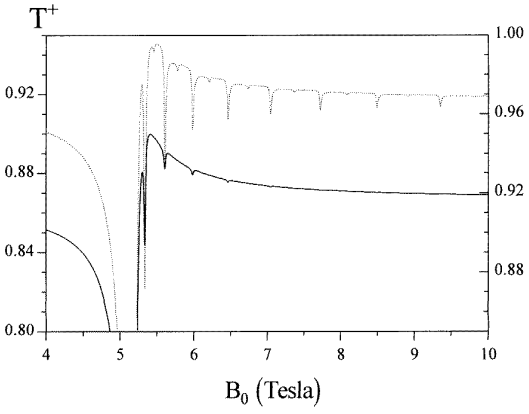

(c)

Figure 9. Field dependence of fixed-frequency transmission through a 50 μm free-standing FeF_2 film with $|\Gamma_\alpha| = |\Gamma_\beta| = 2.0 \times 10^{-4}\omega_m$. Boundary conditions are pinned spin (...) and unpinned spin (——). (a) + and (b) − polarization for $\omega/2\pi c = 57.0\ \text{cm}^{-1} > \omega_R$; (c) + polarization for $\omega/2\pi c = 47.0\ \text{cm}^{-1} < \omega_R$. In (b) and (c) the curves for unpinned spin are referred to the right-hand scale.

− polarization. Figure 8 shows transmission curves with the same parameters as figure 6(a) but in the presence of an applied field. The main difference is the Zeeman splitting, with minor differences between the + and − curves due to the fact that the resonances fall at different points relative to the slowly varying optical-wave fringe background.

It seems likely that frequency-swept spectra will be of most relevance but much magnetic resonance work is done by means of field sweep at fixed frequency so for the sake of completeness we present some spectra of this kind in figure 9. The fringe patterns can be interpreted by reference to the dispersion curves of wave number versus field shown for the spin modes in figures 3(a) and 3(c). For $\omega/2\pi c = 57.0$ cm^{-1} figure 3(a) shows that k_S^+ is real for all B_0 whereas k_S^- is real only up to $B_0 = 4.4$ T. Correspondingly, figure 9(a) shows fringes in T^+ for all B_0 and figure 9(b) shows fringes in T^- only for $B_0 < 4.4$ T. At the lower frequency figure 3(c) has k_S^+ real only for $B_0 > 4.4$ T and k_S^- is never real. Figure 9(c) for T^+ indeed shows fringes only for $B_0 > 4.4$ T. The transmission curve T^- versus B_0 is featureless and is not shown.

5. Conclusions

The main results of this paper are equations (19)–(24) together with the single-interface transmission and reflection coefficients given in the appendix. These give the generalization of the standard calculation presented in I to include dipole-exchange effects. The formalism is general, allowing for the bounding media to be different from one another and including the effect of partial mirrors at the interfaces. As in the pure dipolar case, I, for the Faraday geometry the eigenmodes are the two signs of circular polarization but in this case each polarization has two propagating modes, loosely speaking optical and spin-wave. For the more important case of the antiferromagnet the zero-field transmission and reflection, as seen for example in figure 6, is the same in both polarizations so that the results apply also to unpolarized radiation. Application of a field results in a Zeeman splitting, figure 8 for example, with implications for polarization selection which we have not discussed in any detail.

We have carried out our calculations within a macroscopic formulation of dipole-exchange effects with exchange appearing in the form of $D\nabla^2 M$ terms. This method is widely applied to ferromagnetic film systems and was used in a study of antiferromagnetic films by Stamps and Camley [3]. Our dynamical equations for the antiferromagnet are equivalent to theirs. However, they go on to a detailed study of a different problem, namely the dipole-exchange modes propagating parallel to the film surfaces.

As expected, for a single ferromagnetic film spin-wave fringes resulting from the exchange corrections are very unlikely to be observable. This results from the fact that the thickness of the required film is very small on the scale of the wavelength and it may be that if the calculations are extended to a superlattice the greater magnetic volume of many layers will lead to observable spin-wave fringes.

For antiferromagnets our computed results show that spin-wave fringes large enough to be observable should be present in transmission through films with thicknesses in the right range; this finding is of course what we expected since features due to spin-wave standing modes have been detected in field scans of microwave absorption in epitaxial films of MnF_2 [4]. We stress here the qualitative result, illustrated in figure 6, that the form of the fringes depends strongly on the form of the spin boundary conditions at the interfaces. We have used the Rado–Weertman [2] form of the spin boundary conditions in deriving the transmission and reflection coefficients given in the appendix. These include both pinned- and unpinned-spin conditions as special cases and are therefore adequate to establish the

sensitivity of transmission to the boundary conditions. In some cases, for example two magnetic films in contact, expansion of the equations of motion of interface spins leads to more complicated boundary conditions whose exact form depends on interface exchange and anisotropy coefficients [6, 14]. It appears, therefore, that detailed study of transmission spectra of the kind analysed here may be a means of characterization of antiferromagnetic film systems. Up to now, most applications of magnetic thin films have involved transition-metal ferromagnets for which the frequencies of dipole-exchange guided modes are in an accessible range for Brillouin scattering. Thus the main tool for the determination of interface parameters in ferromagnetic-film systems has been the detailed study by this means of the dynamics of the dipole-exchange modes [15]. Recently, there has been discussion of possible applications of antiferromagnetic films, for example for exchange biasing of sensors and read heads. Antiferromagnetic dipole-exchange modes are at too high a frequency for Brillouin scattering and the question of a viable characterization technique is still open. The analysis and the results that we have presented, taken with the high resolution that has been achieved in recent FIR studies [13], suggest that FIR spectroscopy may be the tool that is needed.

A number of generalizations of the calculations presented here is possible. We have already mentioned the extension to superlattices, which would involve an application of the standard transfer-matrix formalism [16] to include the exchange-induced spatial dispersion that underlies the present work. We have restricted attention to the Faraday geometry, with normal incidence and applied field normal to the Fabry–Pérot interfaces but we could also discuss, for example, the parallel-field Voigt geometry, as was done in I for the purely optical modes, or if necessary oblique incidence. It may be recalled, too, that in uniaxial antiferromagnets the form of the permeability tensor depends on the angle between the static field and the uniaxis [7] so the number of possible extensions is quite large. However, we believe that the formalism and results presented here are sufficient to establish the key points.

Acknowledgments

We are grateful for helpful discussions of the background to this paper with R E Camley, Kamsul Abraha, T J Parker, S R P Smith and R L Stamps. The work was supported by IRPA (Malaysian government) grant 09-02-05-6001.

Appendix. Single-interface coefficients

These coefficients are derived from the boundary conditions $E_\parallel$ continuous, $\Delta H_\parallel$ given by (17) and the Rado–Weertman condition (16). For the upper interface in figure 4 with only e_I incident ($e_{U1} = e_{U2} = 0$) the boundary conditions are

$$1 + \rho_{12} = \tau_{121} + \tau_{122} \tag{A.1}$$

$$q_1 - \rho_{12} q_1 - (q_{21}\tau_{121} + q_{22}\tau_{122}) = \alpha(\tau_{121} + \tau_{122}) \tag{A.2}$$

$$\tau_{121} = -\Delta\tau_{122} \tag{A.3}$$

where

$$\Delta = \left(\frac{k_{22} - \mathrm{i}\xi}{k_{21} - \mathrm{i}\xi}\right)\left(\frac{q_{22}\chi_{22}}{q_{21}\chi_{21}}\right) \tag{A.4}$$

and the q variables are related to the k variables by $q = \mu ck/\omega_m$. Like μ and k, q carries the implied superscript $\pm$. Solution of (A1)–(A3) gives

$$\tau_{121} = \frac{-2\Delta q_1}{-\Delta(q_1 + q_{21}) + q_1 + q_{22} + \alpha(1-\Delta)} \tag{A.5}$$

$$\tau_{122} = \frac{2q_1}{-\Delta(q_1 + q_{21}) + q_1 + q_{22} + \alpha(1-\Delta)} \tag{A.6}$$

$$\rho_{12} = \frac{q_1 - q_{22} + \Delta(q_{21} - q_1) - \alpha(1-\Delta)}{-\Delta(q_1 + q_{21}) + q_1 + q_{22} + \alpha(1-\Delta)}. \tag{A.7}$$

Similar calculations give the other coefficients, which are

$$\rho_{2111} = \frac{q_1(\Delta - \delta) - \Delta q_{21} - \delta q_{22} + \alpha(\Delta - \delta)}{-\Delta(q_1 + q_{21}) + q_1 + q_{22} + \alpha(1-\Delta)} \tag{A.8}$$

$$\rho_{2121} = \frac{q_{21}(1+\delta) - q_1(1-\delta) - \alpha(1-\delta)}{-\Delta(q_1 + q_{21}) + q_1 + q_{22} + \alpha(1-\Delta)} \tag{A.9}$$

$$\tau_{211} = \frac{q_{21} + q_{22} - 2\Delta q_{21} + \delta(q_{21} - q_{22})}{-\Delta(q_1 + q_{21}) + q_1 + q_{22} + \alpha(1-\Delta)} \tag{A.10}$$

$$\rho_{2112} = \frac{q_{22}\Delta(1+\delta) - q_1\Delta(1-\delta) - \alpha\Delta(1-\delta)}{\Delta(q_1 + q_{21}) - (q_1 + q_{22}) + \alpha(\Delta - 1)} \tag{A.11}$$

$$\rho_{2122} = \frac{q_1(1 - \delta\Delta) - q_{22} - \Delta\delta q_{21} + \alpha(1 - \delta\Delta)}{\Delta(q_1 + q_{21}) - (q_1 + q_{22}) + \alpha(\Delta - 1)} \tag{A.12}$$

$$\tau_{212} = \frac{\Delta(q_{21} + q_{22}) - 2q_{22} + \Delta\delta(q_{22} - q_{21})}{\Delta(q_1 + q_{21}) - (q_1 + q_{22}) + \alpha(\Delta - 1)}. \tag{A.13}$$

Coefficients for reflection and transmission at the 2–3 interface are obtained by means of obvious substitutions.

References

[1] Siew-Choo Lim, Osman Junaidah and Tilley D R 1997 *J. Phys.: Condens. Matter* **9** 8297
[2] Rado G and Weertman J R 1959 *J. Phys. Chem. Solids* **11** 315
[3] Stamps R L and Camley R E 1987 *Phys. Rev.* B **35** 1919
[4] Lui M, Ramos C A, King A R and Jaccarino V 1990 *J. Appl. Phys.* **67** 5518
[5] Kalinikos B A 1994 *Linear and Nonlinear Spin Waves in Magnetic Films and Superlattices* ed M G Cottam (Singapore: World Scientific) ch 2
[6] Cottam M G and Tilley D R 1989 *Introduction to Surface and Superlattice Excitations* (Cambridge: Cambridge University Press)
[7] Kamsul Abraha and Tilley D R 1996 *Surf. Sci. Rep.* **24** 125
[8] Cottam M G and Slavin A N 1994 *Linear and Nonlinear Spin Waves in Magnetic Films and Superlattices* ed M G Cottam (Singapore: World Scientific)
[9] Rado G T and Hicken R J 1988 *J. Appl. Phys.* **63** 3885
[10] Heavens O S 1965 *Optical Properties of Thin Solid Films* (New York: Dover)
[11] Landau L D and Lifshitz E M 1960 *Electrodynamics of Continuous Media* (Oxford: Pergamon)
[12] Brown D E, Dumelow T, Parker T J, Abraha K and Tilley D R 1994 *Phys. Rev.* B **49** 12 266
[13] Jensen M R F, Feiven S A, Parker T J and Camley R E 1997 *J. Phys.: Condens. Matter* **9** 7233
[14] Damon R W and Eshbach J R 1961 *J. Phys. Chem. Solids* **19** 308
[15] Demokritov S and Tsymbal E 1994 *J. Phys.: Condens. Matter* **6** 7145
[16] Raj N and Tilley D R 1989 *The Dielectric Function of Condensed Systems* ed L V Keldysh, D A Kirzhnitz and A A Maradudin (Amsterdam: Elsevier) ch 7